INTERNATIONAL JOURNAL FOR NUMERICAL METHODS IN FLUIDS
*Int. J. Numer. Meth. Fluids* 2002; **39**:325–342 (DOI: 10.1002/fld.337)

# A coupled lattice BGK model for the Boussinesq equations☆

Zhaoli Guo[1,*,†], Baochang Shi[2] and Chuguang Zheng[1]

[1]*National Laboratory of Coal Combustion, Huazhong University of Science and Technology, Wuhan 430074, People's Republic of China*
[2]*Department of Mathematics, Huazhong University of Science and Technology, Wuhan 430074, People's Republic of China*

SUMMARY

In this paper, a thermal lattice BGK model is developed for the Boussinesq incompressible fluids. The basic idea is to solve the velocity field and the temperature field using two independent lattice BGK equations, respectively, and then combine them into one coupled model for the whole system. The porous plate problem and the two-dimensional natural convection flow in a square cavity with $Pr = 0.71$ and various of Rayleigh numbers are simulated using the model. The numerical results are found to be in good agreement with the analytical solutions or those of previous studies. Copyright © 2002 John Wiley & Sons, Ltd.

KEY WORDS: lattice BGK method; porous plate problem; natural convection

## 1. INTRODUCTION

Lattice Boltzmann BGK (LBGK) method is a new numerical scheme for simulating viscous compressible flows in the subsonic regime. Instead of solving the usual continuum hydrodynamic equations for the conserved fields, the LBGK method tries to model the fluid flow by tracking the evolution of the distribution functions of the microscopic fluid particles. This kinetic nature of the LBGK method introduces some important features that distinguish it from other numerical methods, such as the easy modeling of interactions among the fluids and full parallelism. In recent years LBGK has achieved great success in simulations of fluid flows and modeling physics in fluids. A recent comprehensive review of this rapid developing area is presented in Reference [1].

Originally, only mass and momentum conservations were considered in the LBGK method. However, in many applications it is important and sometimes critical to consider the thermal effects in fluid flows. LBGK models for thermal fluid flows have been developed by several

☆This work is subsidized by the Special Funds for Major State Basic Research Projects (G1999022207) and the National Natural Science Foundation of China (6073044).
*Correspondence to: Z. Guo, National Laboratory of Coal Combustion, Huazhong University of Science and Technology, Wuhan 430074, People's Republic of China.
†E-mail: pcihust@public.wuhan.cngb.com

*Received January 2000*
*Revised December 2001*

groups. In general, these thermal LBGK models fall into two categories: the multispeed (MS) approach and the multi-distribution function (MDF) approach. The MS approach is a straightforward extension of the isothermal LBGK models in which only the density distribution function is used [2–4]. To obtain the macroscopic energy equation, the MS models introduce some additional discrete velocities and the equilibrium distributions usually include higher order velocity terms. Two limitations in the MS models severely restrict their applications, i.e., the severe numerical instability and the narrow range of temperature variation.

Both limitations of the MDF approach can be partly overcome by the MDF approach. The MDF approach utilizes the fact that, if the viscous heat dissipation and compression work done by the pressure are negligible, the temperature field is passively advected by the fluid flow and obeys a simpler passive-scalar equation. In an MDF model, the temperature equation is also solved using an LBGK equation by introducing an independent distribution function [5]. MDF models can improve the numerical stability and the range of temperature variation. The accuracy of the MDF models has been verified by several benchmark studies [6–8].

Despite the advantages of the MDF models, there are still some limitations. For instance, in order to get the correct macroscopic equations from the MDF models, it must be assumed that the Mach number of the flow is small and the density varies slowly. So theoretically the MDF model can only be used to simulate compressible flows in the incompressible limit. When used for incompressible flows, the method must be viewed as an artificial compressible method. In some cases, such as turbulent flows, this compressibility may produce some undesired unphysical phenomena [9].

Some efforts have been made to reduce or eliminate such errors [10–12] for isothermal LBGK models. Recently, an MDF thermal LBGK model for the Boussinesq equations was presented in Reference [8] based on an incompressible isothermal LBGK model. In a previous work [13], an improved isothermal LBGK which can model the incompressible Navier–Stokes equation was designed for both steady and unsteady flows. In this paper, we extend this incompressible model for thermal fluid flows by introducing an additional LBGK equation using a temperature distribution function to describe the evolution of the temperature field. The temperature distribution is then coupled to the velocity distribution function based on the Boussinesq assumption. We call this model for the whole system a ‘Coupled LBGK’, referred to as CLBGK. The CLBGK is similar to the MDF since both use multiple ‘distribution functions’. However, different ‘distribution functions’ of the conventional MDF models are based on the same lattice, while in the present CLBGK model the velocity and temperature distribution functions can use different lattices. Therefore, the CLBGK is more flexible than the standard MDF models. The rest of the paper is organized as follows. In Section 2, the CLBGK is constructed. In Section 3, numerical simulations are performed for the porous plate problem with temperature gradient and the two-dimensional natural convection flow in a square cavity with two side walls maintained at different temperature. The numerical results are compared with the analytical solutions or those of previous studies using finite difference (FD) or multigrid methods. Some discussions are made in Section 4.

## 2. THE COUPLED LATTICE BGK MODEL

In this section, we will propose a coupled LBGK model in two-dimensional space. The approach can also be used to develop other models either in two- or three-dimensional space.

 

The standard LBGK method based on a square lattice and a recent improved model for incompressible fluid flows are first briefly reviewed, and a simple LBGK equation is then developed using four discrete velocities for the temperature field. Finally, the two LBGK equations are combined up into the CLBGK model based on the Boussinesq assumption.

### 2.1. LBGK equation for velocity field

The LBGK method originates from the lattice gas automata (LGA) method, a simplified fictitious molecular dynamic in which space, time, and particle velocities are all discrete. In the LGA method, the fluid is described by a set of discrete particles residing on a regular lattice. The state of a lattice node is described by a set of Boolean variables $n_i(\mathbf{x},t)$ $(i=0,\ldots,b-1)$ representing the particle occupation, where $b$ is the number of velocity directions of the particle at each node. The particles collide at lattice nodes and move along the links. The fluid density and velocity are determined from the statistic motions of the particles. The LBGK method maintains most of the advantages and remedies many shortcomings of the LGA method. The main feature of the LBGK method different from the LGA method is to replace the Boolean variables $n_i$ by the single-particle distribution function $f_i$, and replace the complicated collision operator of LGA by the simple Bhatnagar–Gross–Krook (BGK) collision operator. Specially, the evolution of LBGK is described by the following equation,

$$f_i(\mathbf{x}+c\mathbf{e}_i\Delta t, t+\Delta t) = f_i(\mathbf{x},t) - \frac{1}{\tau}(f_i - f_i^{(eq)}) \tag{1}$$

where $\mathbf{e}_i$ are the discrete velocity directions, $c=\Delta x/\Delta t$ is the particle speed, $\Delta x$ and $\Delta t$ are the lattice spacing and time increment, respectively. $\tau$ characterizes the relaxation time of the distribution function towards the local equilibrium $f_i^{(eq)}$. The fluid density $\rho$ and velocity $\mathbf{u}$ are determined from the zero and first moments of the distribution functions,

$$\rho = \sum_{i=0}^{b-1} f_i, \quad \rho\mathbf{u} = \sum_{i=0}^{b-1} c\mathbf{e}_i f_i \tag{2}$$

Note that unlike the LGA method, no statistic is needed to calculate the fluid density and velocity in the LBGK method, and therefore statistic noise is completely eliminated. Another distinctive feature of the LBGK method is that the local equilibrium distribution function $f_i^{(eq)}$ can be chosen appropriately to model the correct hydrodynamics in macroscopic limit. Here we choose the two dimensional (D2Q9) model with nine discrete velocity directions based on a square lattice as an example [14]. The discrete velocity directions of D2Q9 are defined by $\mathbf{e}_0=(0,0)$, $\mathbf{e}_i=(\cos(\pi(i-1)/2),\sin(\pi(i-1)/2))$ for $i=1,2,3,4$, and $\mathbf{e}_i=\sqrt{2}(\cos(\pi(i-9/2)/2),\sin(\pi(i-9/2)/2))$ for $i=5,6,7,8$. The equilibrium distribution functions of D2Q9 are given by

$$f_i^{(eq)}(\mathbf{x},t) = \omega_i\rho + \rho s_i(\mathbf{u}(\mathbf{x},t)), \quad \text{for} \quad i=0,1,\ldots,8 \tag{3}$$

where $s_i(\mathbf{u})$ is a function of macroscopic velocity $\mathbf{u}$ and discrete velocity $\mathbf{e}_i$

$$s_i(\mathbf{u}) = \omega_i\left[3\frac{(\mathbf{e}_i\cdot\mathbf{u})}{c} + 4.5\frac{(\mathbf{e}_i\cdot\mathbf{u})^2}{c^2} - 1.5\frac{|\mathbf{u}|^2}{c^2}\right] \tag{4}$$

 

with the weight coefficients $\omega_0 = 4/9$, $\omega_1 = \omega_2 = \omega_3 = \omega_4 = 1/9$, and $\omega_5 = \omega_6 = \omega_7 = \omega_8 = 1/36$. The fluid velocity $\mathbf{u}$ appearing in the above equilibrium distribution function is required to be small enough, i.e. $|\mathbf{u}|/c \approx M \ll 1$, where $M$ is the Mach number.

Through a multiscaling expansion, the mass and momentum equations can be derived from the D2Q9 model as follows [14],

$$\frac{\partial \rho}{\partial t} + \nabla \cdot (\rho \mathbf{u}) = 0 \tag{5}$$

$$\frac{\partial (\rho \mathbf{u})}{\partial t} + \nabla \cdot (\rho \mathbf{u}\mathbf{u}) = -\nabla p + v[\nabla^2(\rho \mathbf{u}) + \nabla(\nabla \cdot (\rho \mathbf{u}))] \tag{6}$$

where $p = c_s^2 \rho$ is the pressure, $c_s = c/\sqrt{3}$ is the sound speed, and the kinematic viscosity is given by

$$v = \frac{(2\tau - 1)}{6} \frac{(\Delta x)^2}{\Delta t} \tag{7}$$

Obviously, if the density fluctuation of the fluid is small enough, or $\rho \approx \rho_0 = \text{constant}$, Equations (5) and (6) become the Navier–Stokes equations for incompressible fluid flows.

From the arguments given above, we can see that the LBGK method can only be viewed as an artificial compressible scheme for solving the incompressible Navier–Stokes equations in the limit where the density goes to a constant. In practical simulations, however, the density cannot be a constant since the pressure is proportional to the density. When used to simulate incompressible flows where the density is a constant, the LBGK solutions might depart from the direct solutions of the incompressible Navier–Stokes equations [9], and at least part of the departures might be attributable to the effects of the compressibility existing in the LBGK method.

Recently, a new LBGK model (ID2Q9) is proposed for incompressible fluid flows [13] where the compressible effects are effectively reduced. The basic idea is to introduce the pressure into the equilibrium distribution functions as an independent variable, and the density does not appear. The discrete velocity directions of the model are the same as used in D2Q9, and a new distribution function $g_i(\mathbf{x}, t)$ is introduced with the equilibrium distribution function $g_i^{(eq)}(\mathbf{x}, t)$ defined by

$$g_i^{(eq)} = \begin{cases} -4\sigma \dfrac{p}{c^2} + s_0(\mathbf{u}) & i = 0 \\ \lambda \dfrac{p}{c^2} + s_i(\mathbf{u}) & i = 1, 2, 3, 4 \\ \gamma \dfrac{p}{c^2} + s_i(\mathbf{u}) & i = 5, 6, 7, 8 \end{cases} \tag{8}$$

where $\sigma$, $\lambda$ and $\gamma$ are parameters satisfying $\lambda + \gamma = \sigma$ and $\lambda + 2\gamma = 1/2$. The evolution equation of ID2Q9 is similar to Equation (1),

$$g_i(\mathbf{x} + c\mathbf{e}_i \Delta t, t + \Delta t) = g_i(\mathbf{x}, t) - \frac{1}{\tau}(g_i - g_i^{(eq)}) \tag{9}$$

 

The primitive macroscopic variables of the compressible fluid, the velocity $\mathbf{u}$ and pressure $p$, are given by

$$u = \sum_{i=1}^{8} c\mathbf{e}_i g_i, \quad p = \frac{c^2}{4\sigma}\left[\sum_{i=1}^{8} g_i + s_0(\mathbf{u})\right] \tag{10}$$

Through multiscaling expansion, the incompressible Navier–Stokes equations can be derived from this incompressible LBGK model as [13]

$$\nabla \cdot \mathbf{u} = 0 \tag{11}$$

$$\frac{\partial \mathbf{u}}{\partial t} + \nabla \cdot (\mathbf{uu}) = -\nabla p + v\nabla^2 \mathbf{u} \tag{12}$$

to the order of $O(\Delta t^2)$ or $O(\Delta x^2)$ if the microscopic velocity $c = O(1)$, where the kinetic viscosity is given by Equation (7).

It should be noted that the physical meaning of the equilibrium distribution function $g_i$ is different from that of the conventional LBGK models. It is rather a *Lagrangian variable* than a distribution function [15], so it can take negative values. Indeed, it can be easily verified that $\sum_{i=0}^{8} g_i^{(eq)} = 0$, and this property plays an important role in deriving the incompressible Navier–Stokes equations. This pressure-representation distribution function is different from the traditional density-representation one, because it may takes negative values. We noticed that a similar distribution function that can take negative values is also used in a two-phase LBGK model [16]. Furthermore, unlike the conventional LBGK model where the pressure is determined by the density through an equation of state for ideal gas, the pressure $p$ defined by Equation (10) is irrelated to the density and can also take negative values, as in many other incompressible Navier–Stokes solvers.

### 2.2. Lattice BGK equation for the temperature field

It is well known that if the viscous heat dissipation and compression work carried out by the pressure are negligible, the temperature field is passively advected by the fluid flow and obeys a simpler passive-scalar equation,

$$\frac{\partial T}{\partial t} + \nabla \cdot (\mathbf{u}T) = \mathscr{D}\nabla^2 T \tag{13}$$

where $\mathscr{D}$ is the diffusivity.

To solve Equation (13) using lattice BGK equation, a lattice with four discrete velocity directions $\mathbf{e}_1, \mathbf{e}_2, \mathbf{e}_3$ and $\mathbf{e}_4$ as defined before is introduced. It should be noted that other lattices, such as the lattice used in the D2Q9 or the FHP model, can also be used. However, it seems that the lattice introduced here is the simplest one.

The lattice BGK equation for Equation (13) is given by

$$T_i(\mathbf{x} + c\mathbf{e}_i\Delta t, t + \Delta t) - T_i(\mathbf{x}, t) = -\frac{1}{\tau'}[T_i(\mathbf{x}, t) - T_i^{(eq)}(\mathbf{x}, t)] \tag{14}$$

 

where $\tau'$ is the dimensionless relaxation time; $T_i$ is the temperature distribution function, and $T_i^{(eq)}$ is the equilibrium value given by

$$T_i^{(0)} = \frac{T}{4}\left[1 + 2\frac{\mathbf{e}_i \cdot \mathbf{u}}{c}\right] \tag{15}$$

The fluid temperature $T$ is calculated from the temperature distribution function

$$T = \sum_{i=1}^{4} T_i \tag{16}$$

It can be shown that the temperature equation (13) can be derived from the lattice BGK equation (14) with Equation (16) through the Chapman–Enskog procedure, a multiscaling expansion technique for solving the Boltzmann equation in kinetic theory. To see this, we first expand $T_i$ as

$$T_i = T_i^{(0)} + \varepsilon T_i^{(1)} + \varepsilon^2 T_i^{(2)} + \ldots \tag{17}$$

where $T_i^{(0)} = T_i^{(eq)}$, and $\varepsilon$ is a small parameter proportion to the Knudsen number (the ratio of the mean free path to the characteristic flow length). In the long-wave-length and low-frequency limit, the lattice spacing $\Delta x$ and the time increment $\Delta t$ can be regarded as small parameters of the same order as $\varepsilon$ [1]. In Equation (17), $f_i^{neq} = \varepsilon T_i^{(1)} + \varepsilon^2 T_i^{(2)} + \cdots$ represents the nonequilibrium part of the distribution function $T_i$ and the following constraints can be derived from Equations (15) and (16):

$$\sum_{i=1}^{4} T_i^{(m)} = 0 \tag{18}$$

for $m = 1, 2, \ldots$

To derive the macroscopic temperature equation, we introduce two macroscopic time scales $t_1 = \varepsilon t$ and $t_2 = \varepsilon^2 t$ and a macroscopic length scale $x_1 = \varepsilon x$, thus

$$\frac{\partial}{\partial t} = \varepsilon \frac{\partial}{\partial t_1} + \varepsilon^2 \frac{\partial}{\partial t_2}, \quad \nabla = \varepsilon \nabla_1 \tag{19}$$

Through a Taylor expansion in time and space, the lattice BGK equation (14) can be written in continuous form as

$$D_i T_i + \frac{\Delta t}{2} D_i^2 T_i + O(\Delta t^2) = -\frac{1}{\tau' \Delta t}(T_i - T_i^{(0)}) \tag{20}$$

where $D_i = (\frac{\partial}{\partial t} + c\mathbf{e}_i \cdot \nabla)$. Substituting Equations (17) and (19) into Equation (20), and collecting the terms of order $\varepsilon$ and $\varepsilon^2$ respectively, we have

$$D_{1i} T_i^{(0)} = -\frac{T_i^{(1)}}{\tau' \Delta t} \tag{21}$$

and

$$\frac{\partial T_i^{(0)}}{\partial t_2} + D_{1i} T_i^{(1)} + \frac{\Delta t}{2} D_{1i} T_i^{(0)} = -\frac{T_i^{(2)}}{\tau' \Delta t} \tag{22}$$

 

where $D_{1i} = (\frac{\partial}{\partial t_1} + c\mathbf{e}_i \cdot \nabla_1)$. By using Equation (21) we can rewrite Equation (22) as

$$\frac{\partial T_i^{(0)}}{\partial t_2} + \left(1 - \frac{1}{2\tau'}\right) D_{1i} T_i^{(1)} = -\frac{T_i^{(2)}}{\tau' \Delta t} \tag{23}$$

Taking summation of Equations (21) and (23) about index $i$, respectively, we can obtain the macroscopic equations on the $t_1$ and $t_2$ time scales:

$$\frac{\partial T}{\partial t_1} + \nabla_1 \cdot (\mathbf{u}T) = 0 \tag{24}$$

and

$$\frac{\partial T}{\partial t_2} + \left(1 - \frac{1}{2\tau'}\right) \nabla_1 \cdot \mathbf{\Pi}^{(1)} = 0 \tag{25}$$

where $\mathbf{\Pi}^{(1)} = \sum_{i=1}^{4} c\mathbf{e}_i T_i^{(1)}$. After some algebra, we have $\mathbf{\Pi}^{(1)} = -\frac{\tau' \Delta x^2}{2\Delta t} \nabla_1 T + O(M^2 \delta T)$, where $\delta T$ is the fluctuation of the fluid temperature which is small for incompressible flows. Combining Equations (24) and (25) we obtain the following temperature equation

$$\frac{\partial T}{\partial t} + \nabla \cdot (\mathbf{u}T) = \mathscr{D} \nabla^2 T \tag{26}$$

to the $O(\Delta t^2)$ order if $M$ is of the same order of $\Delta t$ or higher, where the diffusivity $\mathscr{D}$ is determined by

$$\mathscr{D} = \frac{(2\tau' - 1)}{4} \frac{\Delta x^2}{\Delta t} \tag{27}$$

### *2.3. The coupled lattice BGK model*

The well-known Boussinesq approximation is often used in the study of natural convection. With this approximation, it is assumed that all fluid properties (density, viscosity, thermal diffusivity) can be considered as constant except in the body force term, where the fluid density $\rho$ is assumed to be a linear function of the temperature:

$$\rho = \rho_0 (1 - \beta (T - T_0)) \tag{28}$$

where $\rho_0$ and $T_0$ are the average fluid density and temperature, respectively, $\beta$ is the coefficient of thermal expansion.

With the Boussinesq approximation, the gravity may be rewritten as

$$\mathbf{G} = \rho_0 \mathbf{g} - \rho_0 \mathbf{g} \beta (T - T_0) \tag{29}$$

where $\mathbf{g}$ is the acceleration vector of gravity. After absorbing the first constant part of $\mathbf{G}$ into the pressure term, the Boussinesq equations are obtained:

$$\nabla \cdot \mathbf{u} = 0 \tag{30}$$

$$\frac{\partial \mathbf{u}}{\partial t} + \nabla \cdot (\mathbf{u}\mathbf{u}) = -\nabla p + \nu \nabla^2 \mathbf{u} - \mathbf{g} \beta (T - T_0) \tag{31}$$

 

$$\frac{\partial T}{\partial t} + \nabla \cdot (\mathbf{u}T) = \mathscr{D}\nabla^2 T \tag{32}$$

The Boussinesq equations (30)–(32) can be simulated by the incompressible LBGK equation (9) coupled with the LBGK equation (14) for the temperature field. The coupling is established by adding the following term to the right-hand-side of the evolution equation (9):

$$f_i = -\frac{1}{2c}\Delta t \alpha_i \mathbf{e}_i \cdot \mathbf{g}\beta(T - T_0) \tag{33}$$

where $\alpha_i = \delta_{i2} + \delta_{i4}$.

It should be noted that other forms of $f_i$ can also be used [17]. With this additional term, the incompressible LBGK equation (9) becomes:

$$g_i(\mathbf{x} + c\mathbf{e}_i\Delta t, t + \Delta t) - g_i(\mathbf{x}, t) = -\frac{1}{\tau}[g_i(\mathbf{x}, t) - g_i^{(eq)}(\mathbf{x}, t)] + f_i \tag{34}$$

It can be shown that Equations (30) and (31) can be derived from Equation (34). Finally, Equations (14) and (34) together with Eqs. (5) and (16) constitute a coupled LBGK (CLBGK) model for the Boussinesq equations (30)–(32).

In Reference [8], He *et al.* also proposed a LBGK model for the Boussinesq equations. Although both their model and the present CLBGK one share the same advantages as the MDF ones, it is interesting to make a comparison between these two models. The CLBGK model differs from He's model in several ways. First, the LBGK equation for the velocity field in He' model is based on the isotherm LBGK equation proposed in Reference [12], so the limitations of the isotherm LBGK equation still exist in the thermal model. Namely, the model is still in an artificial compressible form and, as used for unsteady flows, the model requires an additional condition, $T \gg L/c_s$, ($T$ and $L$ are characteristic time and length, respectively) in order to neglect the artificial compressible effect. While the present CLBGK model overcomes these drawbacks. The second difference is that the evolution equation of He's model involves gradient operator, and thus some of the simplicity of the LBGK methods is lost. While the CLBGK model is as simple as the standard LBGK method. The third difference is that in He's model, the distribution function for temperature field is obtained from the distribution function for velocity field, and thus they are required to use the same lattice. While in the present CLBGK model, the distribution function for the temperature field is relatively independent of that for the velocity field, so the CLBGK model can use two independent lattices for the two distribution functions respectively. From this viewpoint, the present CLBGK model is more flexible.

### *2.4. Boundary conditions*

Boundary conditions play important roles in lattice Boltzmann methods in that they will influence the accuracy and stability of the LBM [18, 19]. In a previous study we developed an extrapolation rule for velocity boundary condition [20], which is of second order and has better numerical stability. The method can be easily extended to impose thermodynamic boundary conditions. In our study, we will use this method to implement the velocity and temperature boundary conditions. The basic idea of the extrapolation method is to decompose the distribution function $g_i$ on boundary node $\mathbf{x}_b$ into its equilibrium and nonequilibrium parts:

$$g_i(\mathbf{x}_b, t) = g_i^{(eq)}(\mathbf{x}_b, t) + g_i^{(neq)}(\mathbf{x}_b, t) \tag{35}$$

 

The nonequilibrium term $g_i^{(neq)}$ represents the deviation from the equilibrium which should be small ($|g_i^{(neq)}| \ll |g_i^{(eq)}|$). So it is reasonable to assume that $g_i^{(neq)} = \Delta t g_i^{(1)}$. Thus,

$$g_i^{(neq)}(\mathbf{x}_b, t) = g_i^{(neq)}(\mathbf{x}_f, t) + O(\Delta t^2) = g_i(\mathbf{x}_f, t) - g_i^{(0)}(\mathbf{x}_f, t) + O(\Delta t^2) \tag{36}$$

where $\mathbf{x}_f$ is the nearest neighbour fluid node of $\mathbf{x}_b$.

For velocity boundary condition where velocity $\mathbf{u}(\mathbf{x}_b, t)$ is known and pressure $p(\mathbf{x}_b, t)$ is unknown, the equilibrium part $g_i^{(eq)}(\mathbf{x}_b, t)$ is approximated with a modified equilibrium defined by

$$\bar{g}_i^{(eq)}(\mathbf{x}_b, t) = \begin{cases} -4\sigma \dfrac{p(\mathbf{x}_f, t)}{c^2} + s_0(\mathbf{u}(\mathbf{x}_b, t)) & i = 0 \\ \lambda \dfrac{p(\mathbf{x}_f, t)}{c^2} + s_i(\mathbf{u}(\mathbf{x}_b, t)) & i = 1, 2, 3, 4 \\ \gamma \dfrac{p(\mathbf{x}_f, t)}{c^2} + s_i(\mathbf{u}(\mathbf{x}_b, t)) & i = 5, 6, 7, 8 \end{cases} \tag{37}$$

Note that in incompressible flows the fluctuation of pressure, $\delta p$, is of $M^2$ order, so $p(\mathbf{x}_b, t) = p(\mathbf{x}_f, t) + O(\Delta t M^2)$ and, therefore,

$$g_i^{(eq)}(\mathbf{x}_b, t) = \bar{g}_i^{(eq)}(\mathbf{x}_b, t) + O(\Delta t M^2) \tag{38}$$

In summary, the distribution $g_i(\mathbf{x}_b, t)$ on the boundary node $\mathbf{x}_b$ is calculated as

$$g_i(\mathbf{x}_b, t) = \bar{g}_i^{(eq)}(\mathbf{x}_b, t) + g_i(\mathbf{x}_f, t) - g_i^{(eq)}(\mathbf{x}_f, t) \tag{39}$$

to the accuracy of $O(\Delta t^2 + \Delta t M^2)$, or $O(\Delta t^2)$ if $M \sim \Delta t$.

Thermal boundary conditions can be implemented in a similar way. If the temperature on the boundary node $\mathbf{x}_b$ is known, the temperature distribution is given by

$$T_i(\mathbf{x}_b, t) = T_i^{(eq)}(\mathbf{x}_b, t) + T_i(\mathbf{x}_f, t) - T_i^{(eq)}(\mathbf{x}_f, t) \tag{40}$$

Alternately, if the temperature gradient is known on the boundary node $\mathbf{x}_b$, $T_i(\mathbf{x}_b, t)$ is given by

$$T_i(\mathbf{x}_b, t) = \bar{T}_i^{(eq)}(\mathbf{x}_b, t) + T_i(\mathbf{x}_f, t) - T_i^{(eq)}(\mathbf{x}_f, t) \tag{41}$$

where $\bar{T}_i^{(eq)}(\mathbf{x}_b, t)$ is an approximation to $T_i^{(eq)}(\mathbf{x}_b, t)$ defined by

$$\bar{T}_i^{(eq)}(\mathbf{x}_b, t) = \frac{T(\mathbf{x}_f, t) - (\mathbf{x}_f - \mathbf{x}_b) \cdot \nabla T(\mathbf{x}_b, t)}{4} \left[ 1 + 2 \frac{\mathbf{e}_i \cdot \mathbf{u}(\mathbf{x}_b, t)}{c} \right] \tag{42}$$

It can be easily shown that the boundary conditions, Equations (40) and (41), are both second order in $\Delta t$, or $\Delta x$ if $c = O(1)$.

## 3. SIMULATION RESULTS

To evaluate the performance of the coupled LBGK model developed in the above section, we have carried out numerical simulations for the porous plate problem with a temperature

 

gradient and the natural convection flow in a square cavity. In simulations, the values of the parameters that appeared in the equilibrium used are chosen such that $\lambda : \gamma = \omega_1 : \omega_5$, i.e., which yields $\sigma = 5/12, \lambda = 1/3$, and $\gamma = 1/12$.

### 3.1. Porous plate problem with a temperature gradient

The porous plate problem is a channel flow where the upper cool plate moves with a constant velocity, and a constant normal flow of fluid is injected through the bottom warm plate and withdrawn at the same rate from the upper plate. This problem models a fluid being sheared between two porous plates through which an identical fluid is being injected normal to the shearing direction. The governing equations of the flow in steady state can be written as

$$v_0 \frac{\partial u}{\partial y} = v \frac{\partial^2 u}{\partial y^2} \tag{43}$$

$$\frac{\partial p}{\partial y} = g\beta(T - T_0) \tag{44}$$

$$v_0 \frac{\partial T}{\partial y} = \mathscr{D} \frac{\partial^2 T}{\partial y^2} \tag{45}$$

where $v_0$ is the inject velocity, $T_0 = (T_h + T_c)/2$ is the average of the hot bottom plate temperature $T_h$ and the cool upper plate temperature $T_c$. The analytical solution of the velocity field in steady state is given by [21]:

$$u = u_0 \left( \frac{e^{(Re\ \ y/L)} - 1}{e^{Re} - 1} \right) \tag{46}$$

where $u_0$ is the velocity of the upper plate, $Re$ is the Reynolds number based on the inject velocity $v_0$ and the channel width $L$. The temperature profile in steady state satisfies

$$T = T_0 + \Delta T \left( \frac{e^{(Pr \cdot Re\ \ y/L)} - 1}{e^{Pr \cdot Re} - 1} \right) \tag{47}$$

where $\Delta T = T_h - T_c$ is the temperature difference between the hot and cool walls, $Pr = v/\mathscr{D}$ is the Prandtl number. Another basic characteristic dimensionless parameter of the flow is the Rayleigh number defined by $Ra = g\beta\Delta T L^3/(v\mathscr{D})$.

We first conducted a set of simulations to measure the velocity and temperature profiles for a range of the Reynolds number and Prandtl number. In the simulations, unless otherwise mentioned, the system size is $N_x \times N_y = 64 \times 32$, and the relaxation parameter $\omega = 1/\tau$ is chosen to be 1.25. All other parameters can be chosen in terms of the Reynolds number, Prandtl number and Rayleigh number. Periodic boundary conditions are used at the entrance and exit of the channel, and the velocity and temperature boundary conditions, Equations (39) and (40), are applied to the top and bottom plates.

Figure 1(a) shows the normalized temperature profiles for $Pr = 0.71$, $Ra = 100$ and $Re = 5, 20$ and 30; Figure 1(b) shows the results for $Ra = 100$, $Re = 10$ and $Pr = 0.2$, 0.8 and 1.5. Analytical solutions are also presented for comparison. As shown, the numerical results are in excellent agreement with the analytical solutions. It is also observed that the velocity distribution and the temperature one are both uniform along the channel in all cases.

 

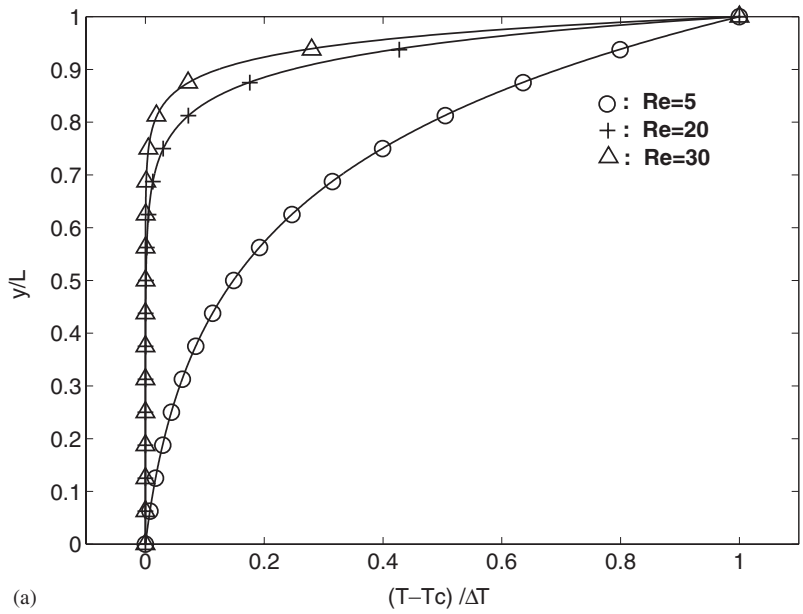


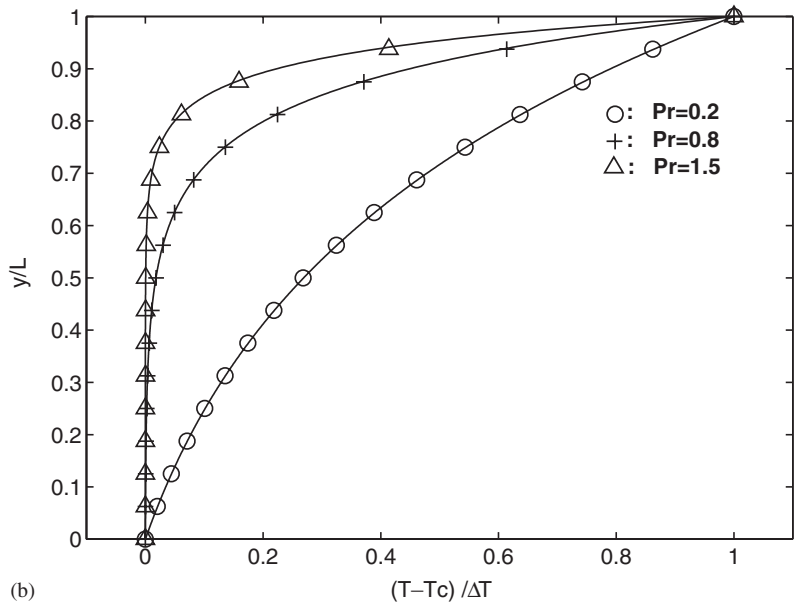


Figure 1. Temperature profiles in the porous plate problem. Solid lines are the analytical solutions, symbols represents the CLBGK solutions. (a) $Pr = 0.71$, $Ra = 100$; and (b) $Ra = 100$, $Re = 10$.

We also tested the ranges of $\tau$ and $\tau'$ applicable for the model. It is well known that the LBGK method will encounter numerical instability as $\tau$ or $\tau'$ are close to 0.5. However, the proposed scheme with the present boundary conditions was found to be accurate and

 

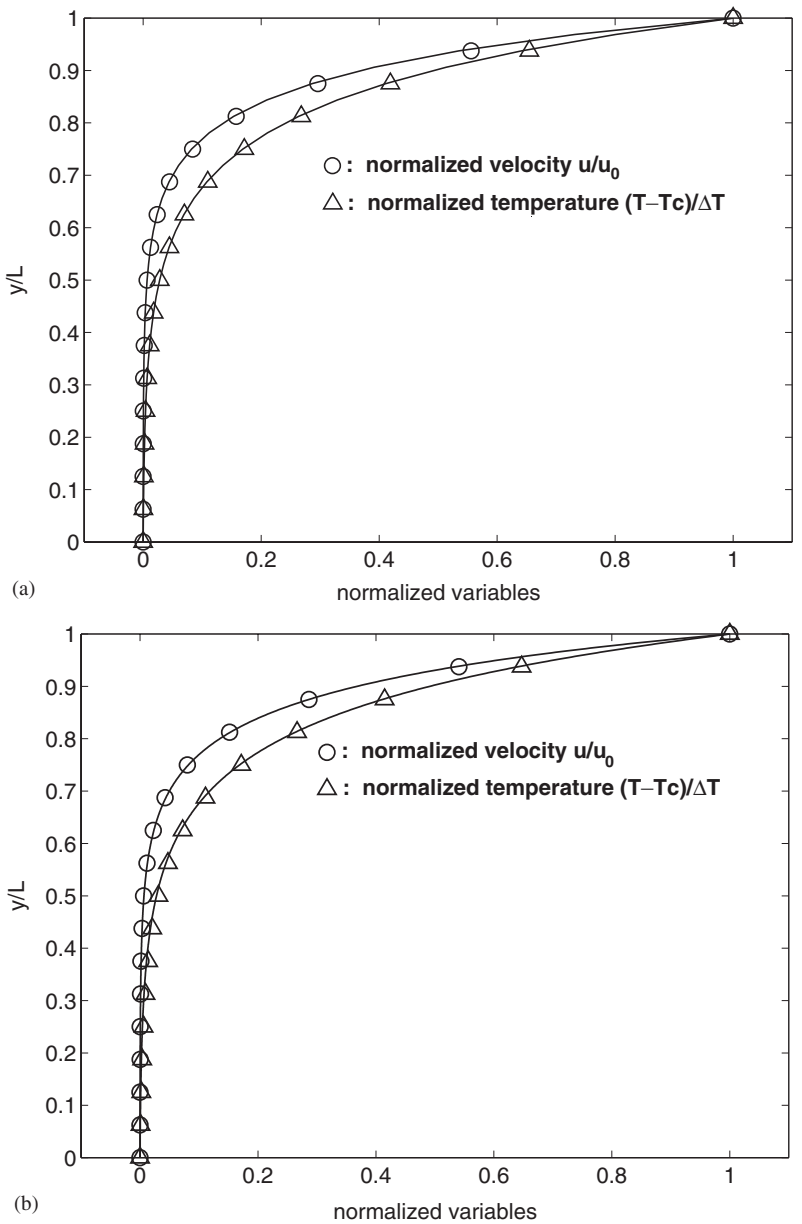


Figure 2. Velocity and temperature profiles in the porpoise plate problem as $Pr = 0.71$, $Re = 10$. Solid lines are the analytical solutions, symbols represents the CLBGK solutions. (a) $1/\tau = 1.99$, $1/\tau' = 1.991$, $Ra = 100$; (b) $\tau = 0.8$, $Ra = 1000$.

stable even as $1/\tau = 1.99$ and $1/\tau' = 1.991$ as $Pr = 0.71$, $Ra = 100$ and $Re = 10$ (see Figure 2(a)). Influence of the Rayleigh number on numerical stability was also studied for $Re = 10$, $Pr = 0.71$ and $\tau = 0.8$. The computations were stable for $Ra = 10$, 100 and 1000

 

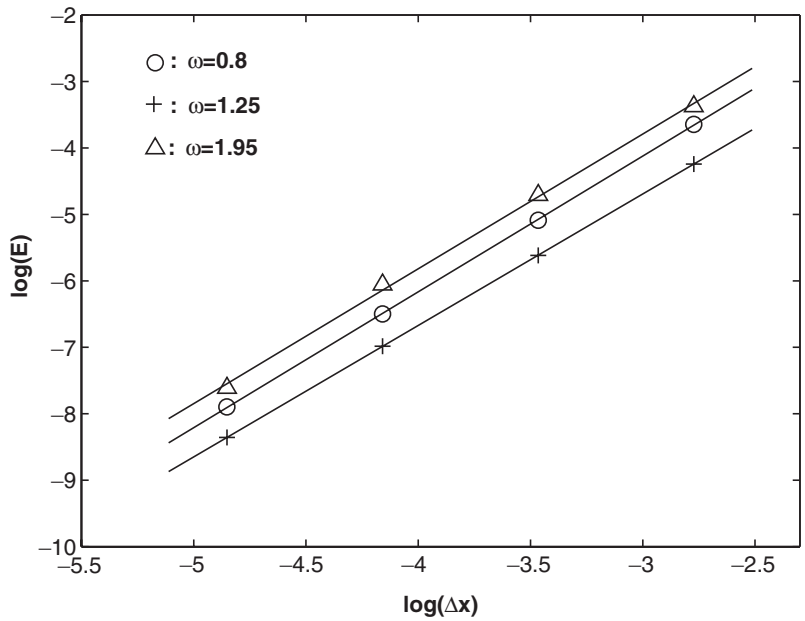


Figure 3. Relative global error versus lattice spacing for the porous plate flow. The slopes of the least-square fitting lines are (○) 2.04, (+) 1.98 and (◇) 2.03, respectively.

(see Figure 2(b)), and the simulation results differ slightly from each other in velocity and temperature fields. It was also found that the relative temperature difference, $(T_h - T_c)/T_c$, has little effect on the accuracy and stability of the computation for a given Rayleigh number considered. As $Ra = 10\ 000$, however, some oscillation occurred during the evolution, and we could not obtain a converged solution.

Simulations were also carried out to evaluate the numerical accuracy of the model. In simulations, the Prandtl number is set to be 0.71, $Re = 10$, and $Ra = 100$. Three different values of relaxation parameter $1/\tau$ (0.8,1.25 and 1.95) were used. In each case, the lattice spacing $\Delta x$ varies from $1/16$ to $1/128$. Relative global errors in temperature field were measure, and are shown in Figure 3 logarithmically. Here the relative global error is defined by [12]:

$$E = \frac{\sqrt{\sum_i |T(\mathbf{x}_i) - T_a(\mathbf{x}_i)|^2}}{\sqrt{\sum_i |T_a(\mathbf{x}_i)|^2}} \tag{48}$$

where the summation is over the entire system, $T_a$ is the analytical solution. In Figure 3, the symbols correspond to the results produced by the present CLBGK scheme, the solid lines are the least-square fittings. The slopes of the solid lines are 2.04, 1.98, and 2.03 for $1/\tau = 0.8, 1.25$ and 1.95, respectively. Clearly the present model is of second order in space.

 

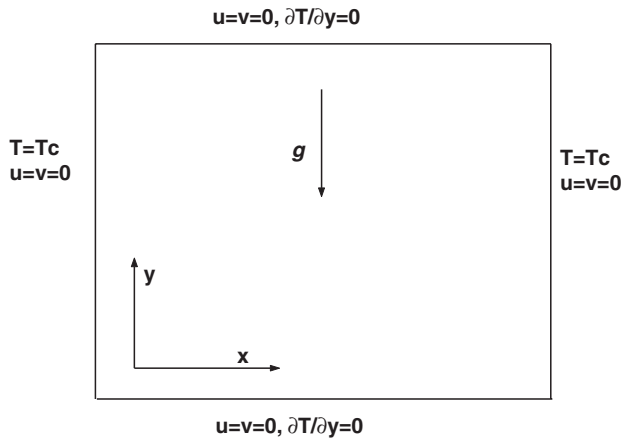


Figure 4. Flow configuration of the natural convection flow.

### 3.2. *Natural convection in a square cavity*

The configuration of the natural convection flow considered consists of a 2-D square cavity with a hot wall on the left side and a cool wall on the right side (see Figure 4). The Rayleigh number of the flow is defined by $Ra = g\beta\Delta TH^3/(v\mathscr{D})$ where $\Delta T$ is the temperature difference between the hot and cool walls, $H$ is the height or width of the cavity.

The natural convection flow in a square cavity has been numerically studied by many authors. A benchmark solution has been published by de Vahl Davis [22]. He used a stream-function-vorticity FD method with meshes up to $81 \times 81$. Another benchmark solution for this problem was presented by Hortmann and Perić using a finite volume multigrid method [23] with much finer grids. In the present paper, simulations for $Ra = 10^3, 10^4, 10^5$, and $10^6$ with the present LBGK model are carried out. In all simulations, $Pr$ is set to be 0.71 (air), and the lattice size used is chosen to be $Nx \times Ny = 128 \times 128$, and the relaxation parameter $\omega = 1/\tau$ is set to be 0.4, 0.5, 1.2 and 1.8 for $Ra = 10^3, 10^4, 10^5$ and $10^6$, respectively. $\omega' = 1/\tau'$ is determined from the Prandtl and Rayleigh numbers. In all simulations the velocity boundary condition, Equation (39), is applied to the four walls, the temperature boundary conditions, Equations (40) and (41), are applied to the vertical walls and horizontal walls, respectively.

Streamlines and isotherms predicted for flows at different Rayleigh numbers are shown in Figures 5(a)–(d) and Figures 6(a)–(d). From the figures, we can see that for low values of $Ra$, a central vortex appears as the typical features of the flow. The vortex tends to become elliptic as $Ra$ increases, and breaks up into two vortices at $Ra = 10^5$. When $Ra$ reaches to $10^6$, the two vortices move towards the walls and a third vortex appears in the center of the cavity. The isotherms show the change of the dominant heat transfer mechanism as the Rayleigh number increases. For small $Ra$, the heat is transferred mainly by conduction between the hot and cold walls, and the isotherms are almost vertical. As $Ra$ increases, the dominant heat transfer mechanism changes from conduction to convection, and the isotherms become horizontal in the center of the cavity, and are vertical only in the thin boundary layers near the hot and cold walls. All of these observations are in good agreement with the results reported in previous studies [23, 24].

 

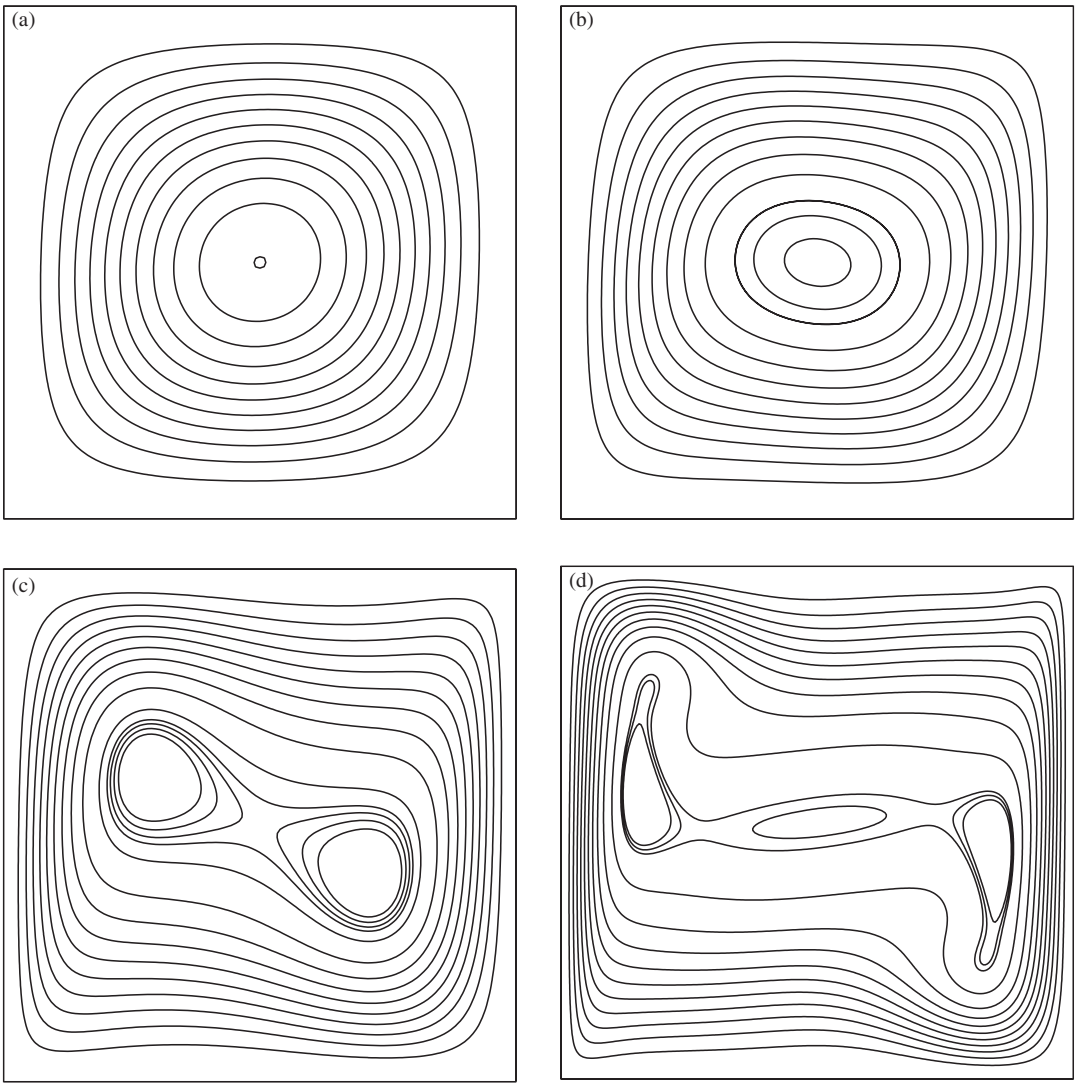


Figure 5. Stream lines of the natural convection flow.

To quantify the results, data of the LBGK solution are listed in Table I as well as the benchmark solution given by Hortmann and Perić [23]. The comparison includes the average Nusselt number $Nu_{\text{ave}}$ along the cold wall, its maximum value $Nu_{\max}$ and the location $y_{Nu}$ where it occurs, the maximum velocity values and their corresponding locations. the maximum horizontal velocity component at the mid-width, $u_{\max}$ and its location $y_{\max}$, and the vertical velocity component at the mid-height, $v_{\max}$ and its location $x_{\max}$. The grid-independent locations $y_{Nu}$, $y_{\max}$ and $x_{\max}$ were not given in Reference [23], and we obtained these data by using the same extrapolation scheme as used in Reference [23]. There is excellent agreement

 

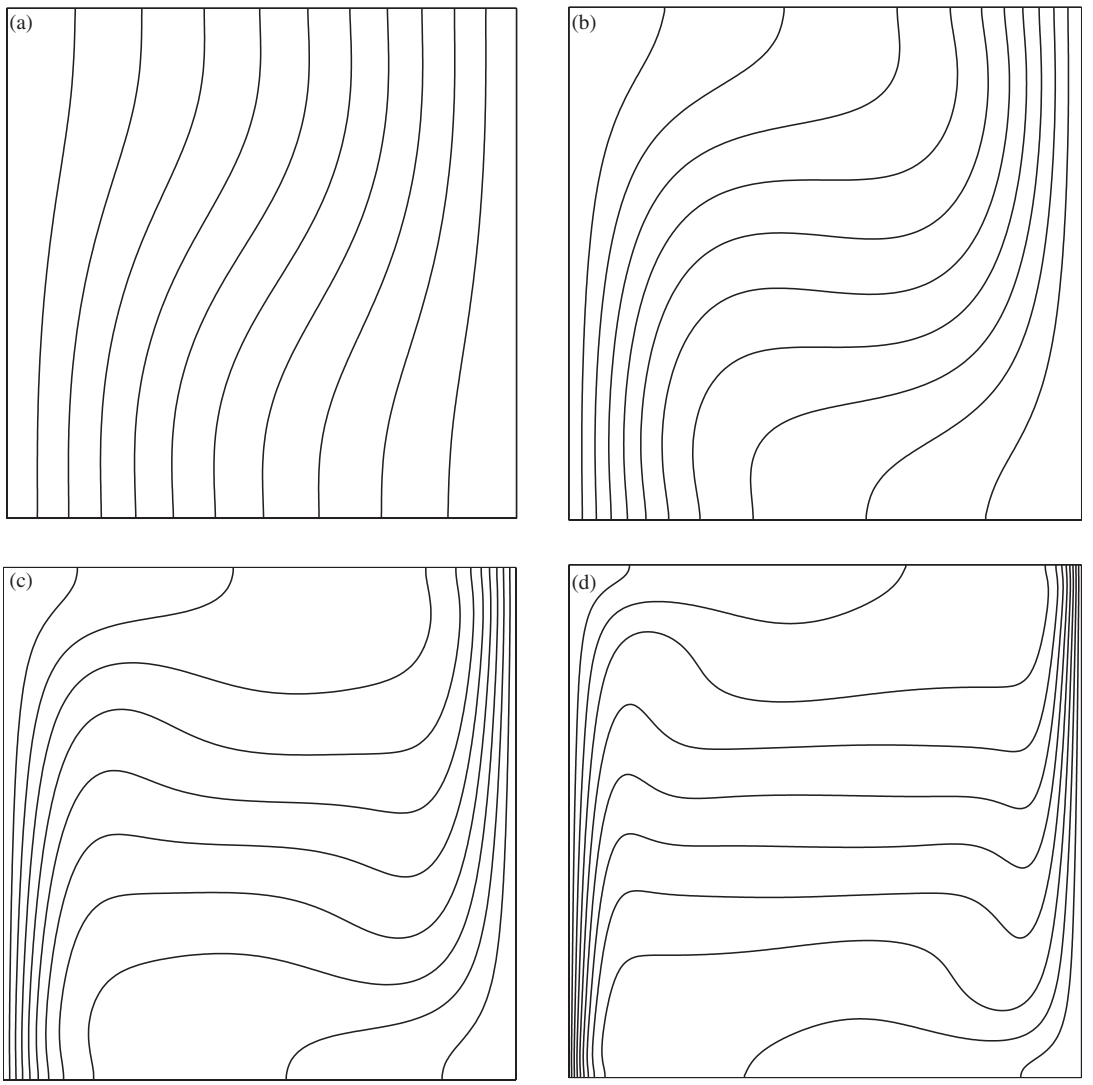


Figure 6. Isotherms of the natural convection flow.

between the two solutions. The difference between the LBGK and the benchmark solutions is less than 2.0 per cent for the Rayleigh numbers considered here.

The relation between $Nu_{\text{ave}}$ and $Ra$ may be described as a power-law equation:

$$Nu_{\text{ave}} = a(Ra)^b$$

where $a$ and $b$ are two constants. The results from the present LBGK simulation give $a = 0.1425$ and $b = 0.2991$, which are in good agreement with the results $(a, b) = (0.143, 0.299)$ reported in Reference [25] and $(a, b) = (0.142, 0.299)$ reported in Reference [24].

 

Table I. Simulation results of the natural convection flow.

| $Ra$ | | $u_{\max}$ | $y_{\max}$ | $v_{\max}$ | $x_{\max}$ | $Nu_{\max}$ | $y_{Nu}$ | $Nu_{\text{ave}}$ |
|---|---|---|---|---|---|---|---|---|
| $10^3$ | a | 3.6554 | 0.8125 | 3.6985 | 0.1797 | 1.5004 | 0.90625 | 1.1168 |
| | b | — | — | — | — | — | — | — |
| $10^4$ | a | 16.0761 | 0.8203 | 19.6368 | 0.1172 | 3.5715 | 0.8594 | 2.2477 |
| | b | 16.1802 | 0.8265 | 19.6295 | 0.1193 | 3.5309 | 0.8531 | 2.2442 |
| $10^5$ | a | 34.8343 | 0.8594 | 68.2671 | 0.0625 | 7.7951 | 0.9219 | 4.5345 |
| | b | 34.7399 | 0.8558 | 68.6396 | 0.0657 | 7.7201 | 0.9180 | 4.5216 |
| $10^6$ | a | 65.3606 | 0.8516 | 216.415 | 0.0391 | 17.4836 | 0.9688 | 8.7775 |
| | b | 64.8367 | 0.8505 | 220.461 | 0.0390 | 17.536 | 0.9608 | 8.8251 |

[a]Present work; [b]benchmark solution [23].

In simulations, the temperature difference seems to have a minor effect on numerical stability in the parameter range considered here. The main parameters affecting the numerical stability are the relaxation times $\tau$ and $\tau'$. We found that the scheme was still accurate and stability even as $1/\tau = 1.99$. For example, as $Ra = 10^6$, the values of $u_{\max}, y_{\max}, v_{\max}, x_{\max}, Nu_{\max}, y_{Nu}$ and $Nu_{\text{ave}}$ are 65.0289, 0.8516, 215.717, 0.0391, 17.391, 0.9688 and 8.7726, respectively, which are within 2.2 per cent departure from the benchmark values.

## 4. CONCLUSIONS

We have presented a coupled LBGK model (CLBGK) for the Boussinesq incompressible flows. Two LBGK equations are first proposed for the velocity and temperature fields, respectively, and then are coupled into a composite model based on the Boussinesq approximation.

Numerical simulations of the porous plate flow with temperature gradient and the natural convection flow in a square cavity were carried out to test the model. For the first problem, the numerical results agree well with the analytical solutions, and the second order accuracy of the model was confirmed. Influences on the numerical stability of the relaxation time $\tau$ and $\tau'$, and the Rayleigh number were also studied.

Simulations of the natural convection flow in a square cavity correctly predicted the flow features for different Rayleigh numbers considered here. The CLBGK solutions compare favorably with the benchmark solutions [23]. The relation between $Nu$ and $Ra$ are also in good agreement with the results of previous studies [24, 25].

The present CLBGK model can be easily extended to other two- or three-dimensional models. Such extension and applications will be considered in future studies.

ACKNOWLEDGEMENTS

The author Zhaoli Guo would like to thank Prof. Yuehong Qian for helpful discussions on the '99 BICCP Workshop on Lattice-Based Method.

 

REFERENCES

1. Chen S, Doolen G. Lattice Boltzmann method for fluid flows. *Annual Review of Fluid Mechanics* 1998; **30**:329–364.
2. Alexander FJ, Chen S, Sterling JD. Lattice Boltzmann thermohydrodynamics. *Physics Review E* 1993; **47**:R2249–2252.
3. Qian Y. Simulating thermohydrodynamics with lattice BGK models. *Journal of Science and Computation* 1993; **8**:231–241.
4. Chen Y, Ohashi H, Akiyama M. Thermal lattice Bhatnagar–Gross–Krook model without nonlinear deviations in macrodynamic equations. *Physics Review E* 1994; **50**:2776–2783.
5. Bartoloni A, Battista C., *et al*. LBE simulations of Rayleigh–Bénard convection on the APE100 parallel processor. *International Journal for Modular Physics C* 1993; **4**:993–1006.
6. Eggles GJM, Somers JA. Numerical simulation of free convective flow using the lattice-Boltzmann scheme. *International Journal of Heat and Fluid Flow* 1995; **16**:357–364.
7. Shan X. Simulation of Rayleigh–Bénard convection using a lattice-Boltzmann method. *Physics Review E* 1997; **55**:2780–2788.
8. He X, Chen S, Doolen GD. A novel thermal model for the lattice Boltzmann method in incompressible limit. *Journal of Computational Physics* 1998; **146**:282–300.
9. Martinez DO, Matthaeus WH, Chen S, Montgomery DC. Comparison of spectral method and lattice Boltzmann simulations of two-dimensional hydrodynamics. *Physics of Fluids* 1994; **6**:1285.
10. Zou Q, Hou S, Chen S, Doolen G. An improved incompressible lattice Boltzmann model for time-independent flows. *Journal of Statistical Physics* 1995; **81**:35–48.
11. Lin Z, Fang H, Tao R. Improved lattice Boltzmann model for incompressible two-dimensional steady flows. *Physics Review E* 1997; **54**:6323–6230.
12. He X, Luo LS. Lattice Boltzmann model for the incompressible Navier–Stoke equation. *Journal of Statistical Physics* 1997; **88**:927–944.
13. Guo Z, Shi B, Wang N. Lattice BGK model for incompressible Navier–Stokes equation. *Journal of Computational Physics* 2000; **165**:288–306.
14. Qian Y, d'Humiéres D, Lallemand P. Lattice BGK models for Navier–Stokes equation. *Europhysics Letters* 1992; **17**:479–484.
15. Ancona GM. Fully Lagrangian and lattice-Boltzmann methods for solving systems of conservation equations. *Journal of Computational Physics* 1994; **115**:107–120.
16. Swift M, Osborn W, Yeomans J. Lattice Boltzmann simulation of nonideal fluids. *Physics Review E* **75**: 830–833.
17. Qian Y, Succi S, Orszag SA. Recent advance in lattice Boltzmann computing. *Annual Reviews of Computational Physics III* 1995; **3**:195–242.
18. Gallivan MA, Noble DR, Georgiads JG, Buckius RO. An evaluation of the bounce-back boundary condition for lattice Boltzmann simulations. *International Journal for Numerical Methods in Fluids* 1997; **25**:249–263.
19. Zou Q, He X. On pressure and velocity boundary conditions for the lattice Boltzmann BGK model. *Physics of Fluids* 1997; **9**:1591–1597.
20. Guo Z, Zheng C, Shi B. An extrapolation method for pressure and velocity boundary conditions in lattice Boltzmann method. *Proceedings of the International Conference on Applied Computational Fluid Dynamics*, Beijing, 2000, pp. 198–202.
21. Noble DR, Chen S, Georgiads JG, Buckius RO. A consistent hydrodynamic boundary condition for the lattice Boltzmann method. *Physics of Fluids* 1995; **7**:203–209.
22. de Vahl Davis G. Natural convection of air in a square cavity: a benchmark numerical solution. *International Journal for Numerical Methods in Fluids* 1983; **3**:249–264.
23. Hortmann M, Perić M. Finite volume multigrid prediction of laminar natural convection: bench mark solutions. *International Journal for Numerical Methods in Fluids* 1990; **11**:189–207.
24. Barakos G, Mitsoulis E, Assimacopoulos D. Natural convection flow in a square cavity revisited: laminar and turbulent models with wall functions. *International Journal for Numerical Methods in Fluids* 1994; **18**: 695–719.
25. Markatos NC, Pericleous KA. Laminar and turbulent natural convection flow in an enclosed cavity. *International Journal of Heat Mass Transfer* 1984; **27**:755–772.

 